Demonstration of Systematic Variation in Human Intraorbital Optic Nerve Size by Quantitative Magnetic Resonance Imaging and Histology

Shaheen Karim,[1,2] *Robert A. Clark,*[1] *Vadims Poukens,*[1] *and Joseph L. Demer*[1,3]

Purpose. To use magnetic resonance imaging (MRI) to measure the diameter along the course of the intraorbital optic nerve in living subjects and cadaveric specimens, and to validate measurements histologically in the same specimens.

Methods. Measurements of the intraorbital optic nerve were made in 23 living human subjects and in three formalin-fixed orbits using high-resolution, surface coil MRI in the coronal plane. Fixed orbits were then serially sectioned in the same plane, and stained by Masson's trichrome for digital morphometry of nerve diameter and densitometry of connective tissue constituents.

Results. In cadaveric specimens, MRI and histologic measurements of optic nerve dimensions were in close quantitative agreement, showing significant decrease in the average optic nerve diameter along its retrobulbar course. This finding was confirmed by MRI in living subjects, with average optic nerve diameter declining from 3.99 ± 0.04 mm (SEM) just posterior to the globe, to 3.50 ± 0.04 mm at 10 mm further to the posterior ($P < 0.0001$). Color densitometry demonstrated a consistent cross-sectional area of nervous tissue, but decreasing amounts of collagen posteriorly.

Conclusions. There is a significant decrease in normal optic nerve diameter along its length in normal subjects, reflecting reduction in connective tissue. High-resolution MRI is a valid and sensitive method of detecting subtle changes in retrobulbar optic nerve size and can be useful in the investigation of structural optic nerve lesions. Optic nerve diameters must be measured, however, at similar distances posterior to the globe to allow meaningful comparisons. (*Invest Ophthalmol Vis Sci.* 2004;45:1047–1051) DOI:10.1167/iovs.03-1246

Given the vast spectrum of congenital malformations and acquired diseases that may afflict the optic nerve, it is not surprising that the optic nerve's physical dimensions have long been the subject of study. Autopsy measurements of retrobulbar optic nerve diameter performed in the early 20th century found average diameters in the range of 3 to 4 mm.[1,2] Such measurements were subject to postmortem shrinkage, among other artifacts, and so had relatively low precision. The need for in vivo diagnostic measurements fueled development of additional techniques for measuring the optic nerve.

Ultrasound has assumed an important role as a convenient and noninvasive method of evaluating structures in the orbit. Standard echography has been used to measure the thickness of the retrobulbar optic nerve and to evaluate its internal reflectivity and structure. With this technique, reported normal mean retrobulbar optic nerve diameters have been in the range of 2.86 to 3.67 mm,[3–5] and optic nerve thickness is reportedly uniform throughout the orbit.[6] Accuracy of ultrasound measurements in the orbit is subject to several limitations, however, including poor penetration of sound waves into the retrobulbar region and the assumption of a constant speed of sound through the orbit, despite the traversing tissues' having different indices of refraction.[7] The accuracy of echographic measurements is also dependent on the angle of incidence of the sound pulse being perpendicular to the structure of interest, a condition that is difficult if not impossible to verify when evaluating structures in the deep orbit.[8]

Magnetic resonance imaging (MRI) provides an alternative mode of orbital imaging that offers numerous advantages, including presumably accurate spatial calibration and excellent resolution in all planes. Using a receiver coil designed for the whole head, investigators have reported a statistically significant decrease in optic nerve diameter from 3.5 ± 0.3 mm (SD) immediately posterior to the globe to 3.1 ± 0.3 mm in midorbit.[9] Neither this observation, nor any other aspect of MRI morphometry of the optic nerve, has been validated by comparison with histologic measurements. Further investigation of quantitative morphometry of the optic nerve is important, with implications in the diagnosis and investigation of many optic nerve diseases.

Using orbital surface coils to achieve superior spatial resolution and digital analysis of histologic and MRI data for quantitative correlation, we studied the size of the optic nerve along its retrobulbar course in normal humans and cadaveric specimens.

Methods

En Bloc Tissue Preparation

Human specimens were obtained from the cadavers of a 17-month-old male (H7), a 44-year-old male (H5), and a 57-year-old female (H8), in conformity with legal requirements and in compliance with the tenets of the Declaration of Helsinki. The orbits of the 17-month-old male and 57-year-old female were obtained from a tissue bank (IIAM, Scranton, PA) in heads fresh frozen shortly after death. The heads were slowly thawed in 10% neutral buffered formalin. The orbit of the 44-year-old male was obtained during authorized autopsy within 24 hours of death.

Magnetic Resonance Imaging

The two cadaveric heads, warmed to body temperature, and the 44-year-old orbit were imaged by MRI in a 1.5-T scanner (Signa; General Electric, Milwaukee, WI) using dual 3-in, phased-array surface coils. Sets of 17 to 20 contiguous quasicoronal image planes, 2 mm in

From the Departments of [1]Ophthalmology and [3]Neurology, David Geffen Medical School at the University of California, Los Angeles, California; and [2]Harvard Medical School, Boston, Massachusetts.

Supported by National Eye Institute Grants EY08313 and EY00331. JLD received an unrestricted award from Research to Prevent Blindness and is the David and Laraine Gerber Professor of Ophthalmology.

Submitted for publication November 14, 2003; revised December 27, 2003; accepted January 5, 2004.

Disclosure: **S. Karim**, None; **R.A. Clark**, None; **V. Poukens**, None; **J.L. Demer**, None

The publication costs of this article were defrayed in part by page charge payment. This article must therefore be marked "*advertisement*" in accordance with 18 U.S.C. §1734 solely to indicate this fact.

Corresponding author: Joseph L. Demer, Jules Stein Eye Institute, 100 Stein Plaza, UCLA, Los Angeles, CA 90095-7002; jld@ucla.edu.

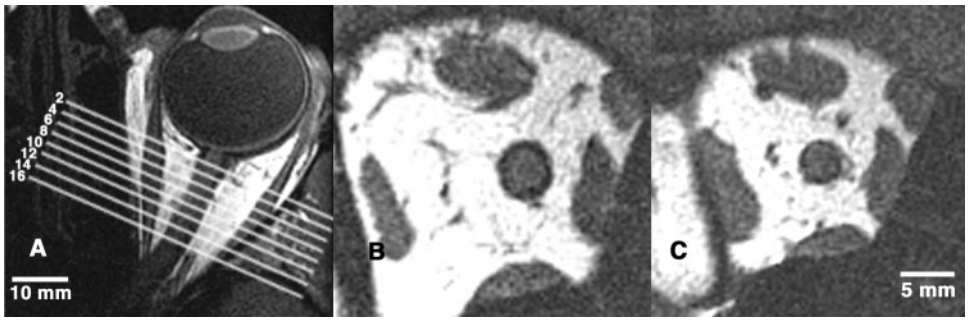

FIGURE 1. Representative axial MRI of orbit (**A**) demonstrates locations of the analyzed quasicoronal image planes (millimeters posterior to junction of globe and optic nerve). Quasicoronal images of the optic nerve are shown in a representative normal subject at 2 (**B**) and 8 (**C**) mm posterior to globe. Identical scale bar for (**B**) and (**C**).

thickness, were obtained with a T1 pulse sequence encompassing a 256 × 256 matrix over a 5-cm^2 field of view (FOV), with four to nine excitations to improve signal-to-noise ratio, resulting in pixel resolution of 195 μm.

After obtaining written informed consent according to a protocol conforming to the Declaration of Helsinki and approved by the Institutional Review Board at the University of California Los Angeles, 23 normal subjects were imaged by MRI, using an array of phased surface coils embedded in a face mask. Sets of 17 to 18 contiguous quasicoronal images, 2 mm in thickness, were then obtained with a T1 pulse sequence (repetition time [TR] of 400–425 ms, echo time [TE] ~20–25 ms, no fat saturation) encompassing a 256 × 256 matrix over an FOV of 8 cm^2, resulting in pixel resolution of 312 μm, except that a 9-cm^2 FOV (351 micron resolution) was used in four subjects and a 6-cm^2 FOV (234-μm resolution) in one subject.

Images were transferred to computers (Macintosh; Apple Computer, Cupertino, CA), converted into eight-bit tagged image file format (TIFF), and quantified by the NIH Image Program (developed by W. Rasband, National Institutes of Health, Bethesda, MD; available by file transfer protocol from zippy.nimh.nih.gov or on floppy disc from NTIS Springfield, VA; catalog number PB95500195GEI).

Quantitative analysis was performed only in MRI images free of motion artifact and in which axial (Fig. 1A) and sagittal reformatting showed that the imaging plane was no more than 20° from transverse to the nerve path throughout its length. Calculations demonstrated that obliquities of nerve path less than 20° would introduce no more than 6% error in measurements, regarded as an acceptable limit.

Further quantitative analysis was performed in 2-mm thickness quasicoronal images obtained in the plane perpendicular to the long axis of the orbit, with reference to image plane zero taken to be that plane closest to the junction of the globe and optic nerve (Fig. 1). After spatial filtering and contrast enhancement in Photoshop image-analysis software (Adobe Systems, Mountain View, CA) to define better the border of the optic nerve against the surrounding cerebrospinal fluid, the optic nerve was outlined within the pia mater using the digital cursor in NIH Image. Images in which the optic nerve was not clearly distinguishable from cerebrospinal fluid were not analyzed. The outline of the optic nerve was used to compute its cross-sectional area, and optic nerve diameter was derived from cross-sectional area, assuming it to be circular. The reproducibility of optic nerve diameter measurements for cadaveric data was estimated by obtaining the SD of calculated diameters for a set of 10 repeated measurements of a representative MRI and histologic section of each specimen.

Histologic Processing and Analysis

The two orbits fixed in situ were then removed intact from the heads, using rongeurs and a high-speed drill under magnification, to thin the orbital bones. As previously described,[10–12] the orbits were decalcified in 0.003 M EDTA and 1.35 N HCl for 24 hours, dehydrated in solutions of alcohol and chloroform or xylenes, embedded in paraffin, and serially sectioned in the coronal plane at a 10-μm thickness. Sections were mounted on 50 × 75-mm gelatin-coated glass slides. Sections 100 to 200 μm apart were processed with Masson trichrome stain to visualize muscle, nerve, and collagen. Care was taken to achieve uniform staining of sections. To maximize chromatic uniformity, sections were processed in batches of 25 to 50 slides.

Digital light micrographs in 24-bit color were made of each orbital section using a microscope (BH-2; Olympus, Tokyo, Japan) fitted with a digital camera (D1X; Nikon, Tokyo, Japan), at a resolution of 3008 × 1960 pixels in 24-bit color. For improved resolution of details, photographs of the optic nerves were also taken using a 2× objective lens, requiring multiple images to be combined in montages seamlessly registered to the individual pixel. Images were sharpened using Photoshop (ver. 6.0; Adobe Systems).

As previously described,[13] stretching and shrinking distortions introduced by histologic processing were corrected by using preprocessed MRIs obtained using absolute spatial scaling. One representative coronal plane MRI that had a comparable histologic section was selected for each of the three specimens. The MRI and histologic images were then superimposed at partial transparency in Photoshop (Adobe Systems) and rotated to identical orientations. The histologic images were then scaled in the horizontal and vertical directions so that orbital walls were superimposed. The shrinkage in orthogonal directions was calculated for each of the three orbits, with mean (±SD) shrinkage of 22% ± 8% × 16% ± 5% (smaller × larger dimension), although it is possible that shrinkage was nonuniform. Calculated optic nerve diameters for that specimen were scaled by the average of the horizontal and vertical shrinkage factors.

Sections stained with Masson trichrome were used to measure optic nerve diameter and collagen and nerve density. Scanned micrographs were analyzed with NIH Image. Optic nerve diameters were calculated using the same method as described for the MRIs, then scaled by a shrinkage correction factor as described earlier. Collagen, constituting the most abundant constituent of the extrafascicular matrix,[14] stains blue with Masson trichrome, while axons and muscle stain red. Using the color range command in Photoshop (Adobe Systems), the blue-staining collagen and purple-staining nerve tissue were independently selected by using a consistent color range across all sections. Collagen and nerve tissue images were then converted into gray scale, imported into NIH Image, and subjected to a consistent binary threshold across all images, and the number of pixels for nerve, collagen, and blank space were counted separately. Percentage area of a component was calculated as the ratio of the number of pixels exceeding threshold for the component divided by the number of pixels exceeding threshold for the image of the whole nerve.

RESULTS

The 23 normal human subjects (12 men, 11 women) ranged in age from 19 to 69 years (33 ± 15, mean ± SD). Optic nerve diameters determined by MRI were computed in the region of 2 to 10 mm posterior to the globe–optic nerve junction, and are plotted in Figure 2.

It is evident from inspection that optic nerve diameter decreased from the anterior to the posterior orbit (Figs. 1B, 1C). Quantitative analysis showed average optic nerve diameter to decrease from 3.99 ± 0.04 mm most anteriorly to 3.50 ± 0.04 mm posteriorly (SEM, range 3.00–4.66 mm, n = 46) in

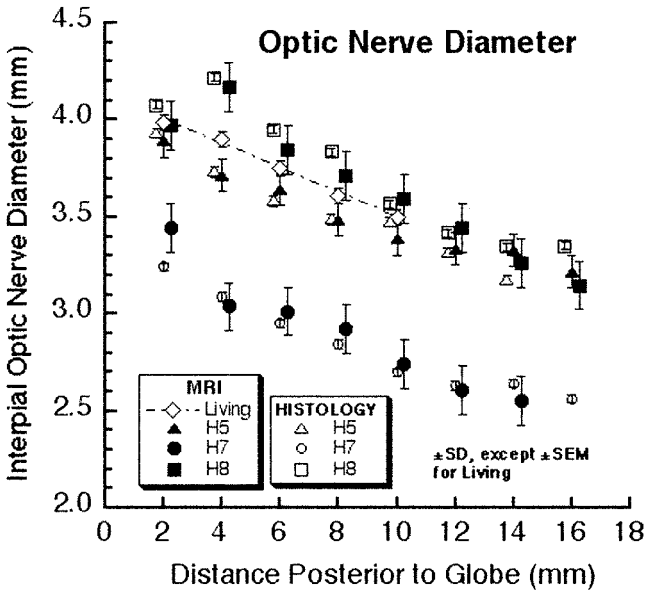

FIGURE 2. Average diameter of optic nerve at different distances posterior to the globe in cadavers and normal subjects, determined by MRI and histologic analysis. Abscissa values are offset by ±0.25 mm for clarity, although all values were measured at 2-mm intervals posterior to globe.

the living subjects. Linear regression through these data points yielded a reasonable fit with slope of -0.0635 ± 0.002 (±SE) that was significantly different from 0.0 ($P < 0.001$), with distance along the orbit accounting for 99% of the variance in optic nerve diameter. Student's paired *t*-test was applied to compare the most anterior and posterior nerve diameters in each orbit, demonstrating a mean difference of 0.495 mm that was significant ($P < 0.0001$). There was no significant difference in optic nerve diameter between the two eyes of individual subjects. The average interocular difference across all pairs of measurements was -0.0079 ± 0.085 mm (±SD, $P > 0.3238$ by two-tailed *t*-test).

For the three cadaveric specimens, stained histologic sections were obtained at intervals of only 100 to 200 μm, facilitating precise pairing of stained sections with corresponding MRI images (Fig. 3). Examination of corresponding MRI and histologic images confirmed the high resolution offered by the former technique.

MRI data were analyzed for distances 2 to 14 mm posterior to the globe optic nerve junction, except for specimen H8, in

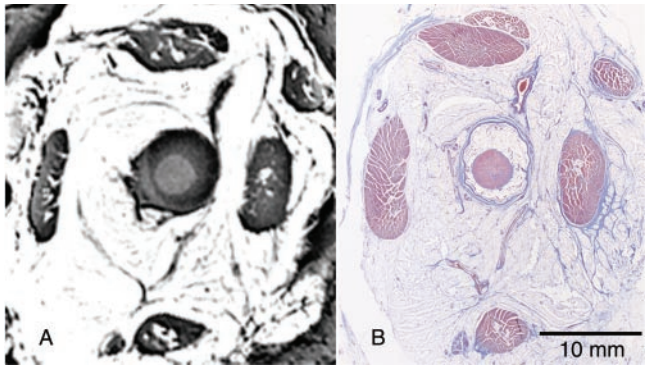

FIGURE 3. MRI of orbit and optic nerve in a 44-year-old cadaveric specimen (H5) at 4 mm posterior to globe (**A**), with its corresponding histologic section stained with Masson's trichrome (**B**). Scale bar is identical for both images.

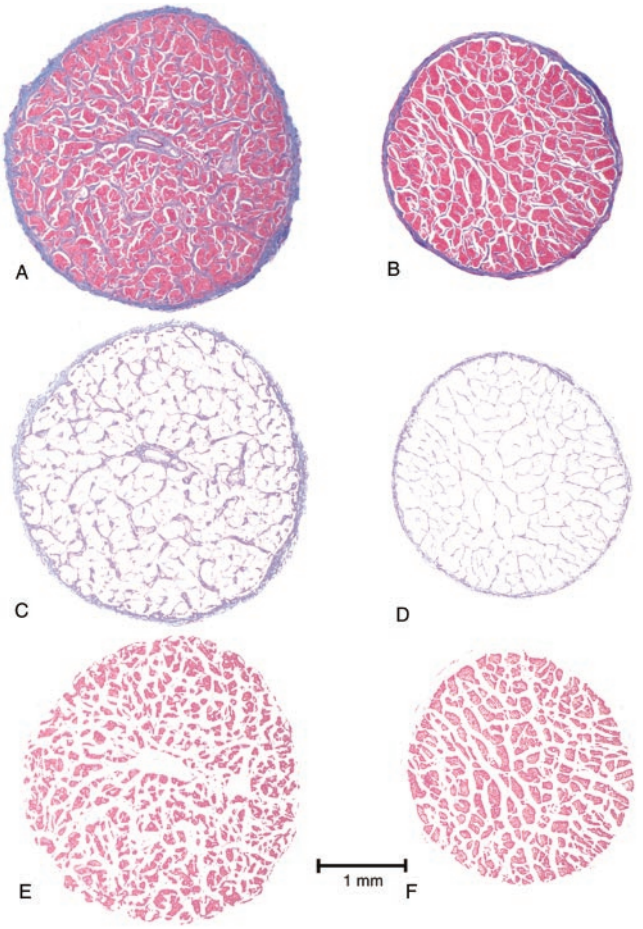

FIGURE 4. Masson's trichrome stained histologic sections of optic nerve from of 17-month-old specimen at 2 (**A**) and 16 (**B**) mm posterior to the globe. Collagen, staining *blue* (**C**, **D**), as well as nerve components, staining *red* (**E**, **F**), were independently selected for quantification.

which case MRIs were interpretable to 16 mm posterior. All three cadaveric specimens demonstrated decreases in optic nerve diameters that mirrored the intraorbital changes observed in the MRIs of living subjects. The relationship of optic nerve diameter to distance posterior to the globe–optic nerve junction is displayed for the cadaveric specimens in Figure 2. Linear regressions through the three cadaveric MRI data sets yielded an average slope (± SEM) of -0.061 ± 0.01, with each slope differing significantly from 0.0 ($P < 0.01$). Similarly, linear regressions for the three histologic data sets yielded an average slope of -0.0578 ± 0.01, with each slope differing significantly from 0.0 ($P < 0.01$). Standard deviations for MRI and histologic determinations of optic nerve diameters in cadaveric specimens did not exceed 0.107 and 0.009 mm, respectively. Histologic determinations of optic nerve diameters were within the SD of MRI measurements in most cases, with an average difference between histologic and MRI measurements of 0.066 mm and a maximum difference of 0.157 mm.

In histologic sections, collagen and nerve tissue could be differentiated readily by the blue stain of the former and purple stain of the latter. Inspection of histologic images suggested that the amount of connective tissue declined posteriorly (Fig. 4). To test the hypothesis that changes in the quantity of collagen could account for the observed changes in retrobulbar optic nerve diameter, densitometry for collagen and nerve tissue was performed in stained sections of specimen H7.

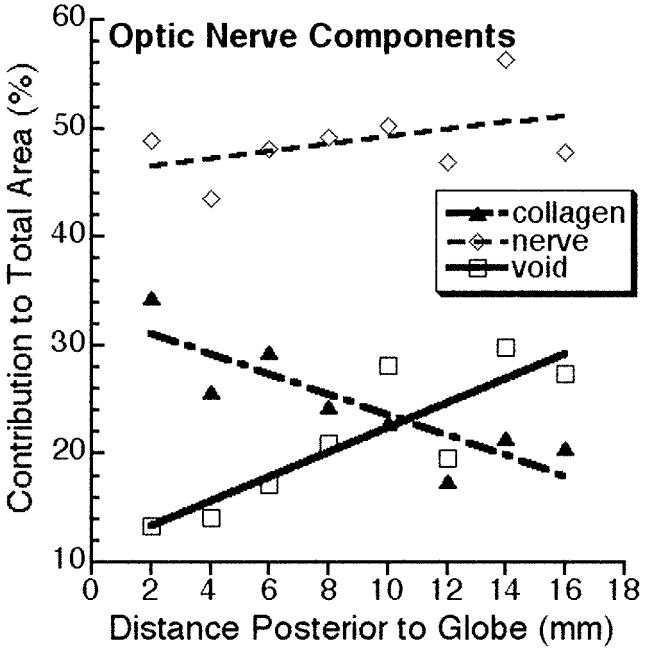

FIGURE 5. Percentage of optic nerve cross-sectional areas constituted by collagen, nerve, and void in a 17-month-old specimen, as a function of distance from the globe.

In Figure 5, the percentages of optic nerve area contributed by collagen and nerve are plotted as functions of distance posterior to the globe–optic nerve junction. In addition, areas of void in the optic nerves, presumably stemming from fluid cavities or processing artifacts, were also determined.

The percentage of nervous tissue was independent of distance from the globe, with a linear regression yielding a slope that was not significantly different from zero ($P > 0.275$). In contrast, a linear fit of the trend for collagen content yielded a slope of -0.9% cross sectional area change/mm ($P < 0.01$), indicating a significant decrease in collagen from anterior to posterior in the optic nerve. The percentage of void space demonstrated a significant increase ($P < 0.01$) from anterior to posterior. Collagen was the only measured component that significantly decreased from anterior to posterior in the orbit. The validity of this component analysis was verified by summing the three measured components in each section. This yielded an average cumulative percentage (±SD) of 94% ± 8% (range, 84–107%). This small deviation from a 100% sum is likely the consequence of a small number of pixels in each tissue component, and omission of border pixels based on the thresholding approach used for tissue image segmentation. The histologic sections of the other two cadaveric specimens subjectively demonstrated the same trends of decreasing collagen posteriorly, with constant nerve content, but had inadequate color separation for densitometric analysis.

DISCUSSION

In the present study of 23 living humans, high-resolution MRI demonstrated a significant decrease in the average optic nerve diameter along its intraorbital course. Comparison of histologic data with MRIs from cadaveric human specimens quantitatively confirmed both this trend of decreasing intraorbital nerve diameter, as well as the validity and sensitivity of orbital MRI to detect subtle changes in optic nerve size. Quantitative analysis applied to modern imaging and histologic methods has permitted us to visualize subtle but statistically significant changes in intraorbital optic nerve diameter that had not been fully appreciated in prior MRI, echographic, or anatomic studies.

The current values of mean optic nerve diameter of 3.50 to 3.99 mm in normal subjects are slightly larger than those published in previous MRI and echographic studies. Using MRI, Lam et al.[15] found mean nerve diameters of 2.6 to 3.3 mm from posterior to anterior, whereas studies using echography have reported optic nerve diameters in normal subjects that range from 2.86 to 3.67 mm.[3–5] The modest discrepancy between the present and prior findings is likely due to superior MRI resolution attained in this study compared with previous investigations, as well as the intrinsic sources of variability in ultrasound described earlier.

Gross observation of the histologic specimens led to the hypothesis that variable amounts of extrafascicular matrix could account for the decreasing optic nerve diameter, a hypothesis supported by the results of the collagen and nerve densitometry. Limitations of the digital analysis techniques used include the use of a threshold to select color ranges and count pixels. Despite the limitations of the densitometric method used, however, our calculation that the nerve compartment is constant in area is consistent with current understanding of axonal anatomy, and the finding of variable amounts of collagen along the length of the nerve is consistent with the subjective appearance of the sections. Furthermore, other investigators have reported systematic changes in the number of fascicles in human optic nerves that would seem to support our hypothesis, with peak counts directly behind the globe, and a nadir in the midorbital region before peaking again in the intracanicular segment.[14] We propose that an increased amount of collagen near the globe is a plausible explanation for the optic nerve diameter phenomenon observed and that it may play an important role in providing additional structural integrity to a region that is subject to numerous mechanical stresses.

As a sensitive measure of retrobulbar optic nerve diameter, high-resolution orbital MRI may serve as a valuable tool in the investigation of tumors, congenital neuropathies, and acquired neuropathies, although care must be taken to measure the optic nerve diameter at similar locations posterior to the globe. In the case of optic nerve gliomas, high-resolution MRI should provide the resolution necessary to better define the precise location and progression of a tumor along the intraorbital nerve. Enhancement of optic nerve gliomas by contrast is variable,[16] making high-resolution imaging particularly useful for small lesions, or when little to no enhancement occurs.

Determination of intraorbital optic nerve diameter by MRI as performed in this study may also aid in the diagnosis of optic nerve hypoplasia (ONH). The diagnosis of ONH is normally made on the basis of the clinical finding of an abnormally small optic nerve head. Ultrasound and fundus photography have been proposed to help confirm the diagnosis, however, because of the imprecision of ophthalmoscopic measurements. Optic nerve measurements from fundus photography are also made more difficult, though, by the requirement that calculations account for the refractive error and axial length of the child's eye.[17,18] MRI of the intracranial segment of the optic nerve has demonstrated a high correlation between diameter of the intracranial nerve and size of the optic disc in patients with ONH.[19] MRI techniques to measure the dimensions of the intraorbital optic nerve diameter could also be used to help confirm the diagnosis of ONH based on comparison of the suspected eye with dimensions of the fellow nerve or normative data presented herein if bilateral involvement is suspected.

Optic nerve imaging by MRI could be useful to diagnose and investigate the pathophysiology of acquired neuropathies such as glaucoma. Ultrasound studies have found significantly decreased optic nerve diameters in patients with advanced glau-

comatous optic neuropathy, leading investigators to propose that echographic measurements of optic nerve diameter might be useful in the assessment of patients with suspected glaucoma.[3] Given this report's findings of decreasing collagen along the intraorbital nerve length, high-resolution MRI may also be informative about the possible role of connective tissues in the pathogenesis of glaucoma. Abnormalities in connective tissue structure and function in the regions of the optic nerve head and lamina cribrosa have been proposed to be involved in the pathogenesis of glaucomatous nerve cupping.[20,21]

Acknowledgments

The authors thank Nicolasa de Salles and Frank Henriquez for valuable technical assistance.

References

1. Hervouët F. Embryologie du nerf optique: le dévelopment postnatal". In: Dejean C, Leplat G, Hervouët F, ed. *L'Embryologie de l'Oeil et sa Tératologie.* Paris: Masson; 1958:171–219.
2. Vierordt H. *Anatomische Physiologische und Physikalische Daten und Tabellan.* Jena, Germany: Fischer, 1906.
3. Beatty S, Good PA, McLaughlin J, O'Neill EC. Echographic measurements of the retrobulbar optic nerve in normal and glaucomatous eyes. *Br J Ophthalmology*. 1998;82:43–47.
4. Skalka HW. Ultrasonography of the optic nerve. In: Smith JL, ed. *Neuro-ophthalmology Update.* New York: Masson; 1977:119–130.
5. Gans MS, Byrne SF, Glaser JS. Standardized A-scan echography in optic nerve disease. *Arch Ophthalmol*. 1987;105:1232–1236.
6. Ossoenig KC, Cennamo G, Byrne SF. Standardized echography of the optic nerve. In: Till P, ed. *Ophthalmic Echography.* Vol. 13. Dordrecht, The Netherlands: Kluwer Academic Publishers; 1993:3–99.
7. Baum G. *Fundamentals of Medical Ultrasonography.* New York: Putnam; 1975.
8. Demer JL, Kerman BM. Comparison of standardized echography with magnetic resonance imaging to measure extraocular muscle size. *Am J Ophthalmol*. 1994;118:351–361.
9. Votruba M, Leary S, Losseff N, et al. MRI of the intraorbital optic nerve in patients with autosomal dominant optic atrophy. *Neuroradiology*. 2000;42:180–183.
10. Demer JL, Miller JM, Poukens V, Vinters HV, Glasgow B. Evidence for fibromuscular pulleys of the recti extraocular muscles. *Invest Ophthalmol Vis Sci*. 1995;36:1125–1136.
11. Demer JL, Oh SY, Poukens V. Evidence for active control of rectus extraocular muscle pulleys. *Invest Ophthalmol Vis Sci*. 2000;41:1280–1290.
12. Demer JL, Poukens V, Miller JM, Micevych P. Innervation of extraocular pulley smooth muscle in monkeys and humans. *Invest Ophthalmol Vis Sci*. 1997;38:1774–1785.
13. Demer JL, Kono R, Poukens V. Quantitative analysis of the structure of the human extraocular muscle pulley system. *Invest Ophthalmol Vis Sci*. 2002;13:2923–2932.
14. Jeffery G, Evans A, Albon J, et al. The human optic nerve: fascicular organisation and connective tissue types along the extra-fascicular matrix. *Anat Embryol*. 1995;191:491–502.
15. Lam BL, Glasier CM, Feuer WJ. Subarachnoid fluid of the optic nerve in normal adults. *Ophthalmology*. 1997;104:1629–1633.
16. Dipaolo DP, Zimmerman RA, Rorke LB. Neurofibromatosis type 1:Pathologic substrate of high-signal-intensity foci in the brain. *Radiology*. 1995;195:721–724.
17. Bengtsson B, Krakau C. Correction of optic disc measurements on fundus photographs. *Graefes Arch Clin Exp Ophthalmol*. 1992;230:24–28.
18. Bengtsson B, Krakau C. Some essential optical features of the Zeiss fundus camera. *Acta Ophthalmol* (*Copenh*). 1977;55:123–131.
19. Hellstrom A, Wiklund LM, Svensson E. Diagnostic value of magnetic resonance imaging and planimetric measurement of optic disc size in confirming ONH. *J AAPOS*. 1999;3:104–108.
20. Morrison JC, Dorman-Pease ME, Dunkelberger GR, Quigley HA. Optic nerve head extracellular matrix in primary optic atrophy and experimental glaucoma. *Arch Ophthalmol*. 1990;108:1020–1024.
21. Quigley HA, Dorman-Pease ME, Brown AE. Quantitative study of collagen and elastin of the optic nerve head and sclera in human and experimental monkey glaucoma. *Curr Eye Res*. 1991;10:877–888.